

# Parasitic loss suppression in photonic and plasmonic photovoltaic light trapping structures

Yi Zou,<sup>1</sup> Xing Sheng,<sup>2</sup> Kun Xia,<sup>1</sup> Huayu Fu,<sup>1</sup> and Juejun Hu<sup>1,\*</sup>

<sup>1</sup>Department of Materials Science & Engineering, University of Delaware, Newark, Delaware, 19716, USA

<sup>2</sup>Department of Materials Science and Engineering, University of Illinois at Urbana-Champaign, Urbana, Illinois, 61801, USA

\*[hujuejun@udel.edu](mailto:hujuejun@udel.edu)

**Abstract:** In this paper, we examine the optical loss mechanisms and mitigation strategies in classical photovoltaic light trapping structures consisting of diffractive gratings integrated with a backside reflector, which couple normal incident solar radiation into guided modes in solar cells to enhance optical absorption. Parasitic absorption from metal or dielectric backside reflectors is identified to be a major loss contributor in such light trapping structures. We elucidate the optical loss mechanism based on the classical coupled mode theory. Further, a spacer design is proposed and validated through numerical simulations to significantly suppress the parasitic loss and improve solar cell performance.

©2014 Optical Society of America

**OCIS codes:** (350.6050) Solar energy; (230.1480) Bragg reflectors; (230.1950) Diffraction gratings; (160.3900) Metals; (240.6680) Surface plasmons.

---

## References and links

1. A. Goetzberger and C. Hebling, "Photovoltaic materials, past, present, future," *Sol. Energy Mater. Sol. Cells* **62**(1-2), 1–19 (2000).
2. P. Bermel, C. Luo, L. Zeng, L. C. Kimerling, and J. D. Joannopoulos, "Improving thin-film crystalline silicon solar cell efficiencies with photonic crystals," *Opt. Express* **15**(25), 16986–17000 (2007).
3. J. Muller, B. Rech, J. Springer, and M. Vanecek, "TCO and light trapping in silicon thin film solar cells," *Sol. Energy* **77**(6), 917–930 (2004).
4. S. Pillai, K. R. Catchpole, T. Trupke, and M. A. Green, "Surface plasmon enhanced silicon solar cells," *J. Appl. Phys.* **101**(9), 093105 (2007).
5. J. Zhu, C. M. Hsu, Z. F. Yu, S. H. Fan, and Y. Cui, "Nanodome Solar Cells with Efficient Light Management and Self-Cleaning," *Nano Lett.* **10**(6), 1979–1984 (2010).
6. J. G. Mutitu, S. Y. Shi, C. H. Chen, T. Creazzo, A. Barnett, C. Honsberg, and D. W. Prather, "Thin film solar cell design based on photonic crystal and diffractive grating structures," *Opt. Express* **16**(19), 15238–15248 (2008).
7. D. Y. Zhou and R. Biswas, "Photonic crystal enhanced light-trapping in thin film solar cells," *J. Appl. Phys.* **103**(9), 093102 (2008).
8. C. Battaglia, J. Escarre, K. Soderstrom, M. Charriere, M. Despeisse, F. J. Haug, and C. Ballif, "Nanomoulding of transparent zinc oxide electrodes for efficient light trapping in solar cells," *Nat. Photonics* **5**(9), 535–538 (2011).
9. H. A. Atwater and A. Polman, "Plasmonics for improved photovoltaic devices," *Nat. Mater.* **9**(3), 205–213 (2010).
10. N. N. Feng, J. Michel, L. Zeng, J. Liu, C. Y. Hong, L. C. Kimerling, and X. Duan, "Design of highly efficient light-trapping structures for thin-film crystalline silicon solar cells," *IEEE Trans. Electron. Dev.* **54**(8), 1926–1933 (2007).
11. X. Sheng, J. F. Liu, I. Kozinsky, A. M. Agarwal, J. Michel, and L. C. Kimerling, "Design and Non-Lithographic Fabrication of Light Trapping Structures for Thin Film Silicon Solar Cells," *Adv. Mater.* **23**(7), 843–847 (2011).
12. L. Zeng, P. Bermel, Y. Yi, B. A. Alamariu, K. A. Broderick, J. Liu, C. Hong, X. Duan, J. Joannopoulos, and L. C. Kimerling, "Demonstration of enhanced absorption in thin film Si solar cells with textured photonic crystal back reflector," *Appl. Phys. Lett.* **93**(22), 221105 (2008).
13. Z. F. Yu, A. Raman, and S. H. Fan, "Fundamental limit of nanophotonic light trapping in solar cells," *Proc. Natl. Acad. Sci. U.S.A.* **107**(41), 17491–17496 (2010).
14. S. E. Han and G. Chen, "Toward the Lambertian Limit of Light Trapping in Thin Nanostructured Silicon Solar Cells," *Nano Lett.* **10**(11), 4692–4696 (2010).
15. Z. F. Yu, A. Raman, and S. H. Fan, "Fundamental limit of light trapping in grating structures," *Opt. Express* **18**(S3 Suppl 3), A366–A380 (2010).

16. Z. C. Holman, S. De Wolf, and C. Ballif, "Improving metal reflectors by suppressing surface plasmon polaritons: a priori calculation of the internal reflectance of a solar cell," *Light Sci. Appl.* **2**, e106 (2013).
17. X. Sheng, J. F. Liu, N. Coronel, A. M. Agarwal, J. Michel, and L. C. Kimerling, "Integration of Self-Assembled Porous Alumina and Distributed Bragg Reflector for Light Trapping in Si Photovoltaic Devices," *IEEE Photon. Technol. Lett.* **22**(18), 1394–1396 (2010).
18. L. Zeng, Y. Yi, C. Hong, J. Liu, N. Feng, X. Duan, L. C. Kimerling, and B. A. Alamariu, "Efficiency enhancement in Si solar cells by textured photonic crystal back reflector," *Appl. Phys. Lett.* **89**(11), 111111 (2006).
19. J. N. Winn, Y. Fink, S. H. Fan, and J. D. Joannopoulos, "Omnidirectional reflection from a one-dimensional photonic crystal," *Opt. Lett.* **23**(20), 1573–1575 (1998).
20. X. Sheng, S. G. Johnson, L. Z. Broderick, J. Michel, and L. C. Kimerling, "Integrated photonic structures for light trapping in thin-film Si solar cells," *Appl. Phys. Lett.* **100**(11), 111110 (2012).
21. H. W. Deckman, C. R. Wronski, H. Witzke, and E. Yablonovitch, "Optically enhanced amorphous-silicon solar-cells," *Appl. Phys. Lett.* **42**(11), 968–970 (1983).
22. S. S. Hegedus and R. Kaplan, "Analysis of quantum efficiency and optical enhancement in amorphous Si p-i-n solar cells," *Prog. Photovolt. Res. Appl.* **10**(4), 257–269 (2002).
23. N. N. Lal, H. Zhou, M. Hawkeye, J. K. Sinha, P. N. Bartlett, G. A. J. Amaratunga, and J. J. Baumberg, "Using spacer layers to control metal and semiconductor absorption in ultrathin solar cells with plasmonic substrates," *Phys. Rev. B* **85**(24), 245318 (2012).
24. J. Morris, R. R. Arya, J. G. Odowd, and S. Wiedeman, "Absorption enhancement in hydrogenated amorphous silicon-based solar-cells," *J. Appl. Phys.* **67**(2), 1079–1087 (1990).
25. S. Pillai, F. J. Beck, K. R. Catchpole, Z. Ouyang, and M. A. Green, "The effect of dielectric spacer thickness on surface plasmon enhanced solar cells for front and rear side depositions," *J. Appl. Phys.* **109**(7), 073105 (2011).
26. J. Gjessing, A. S. Sudbo, and E. S. Marstein, "Comparison of periodic light-trapping structures in thin crystalline silicon solar cells," *J. Appl. Phys.* **110**(3), 033104 (2011).

## 1. Introduction

Currently more than 90% of the global photovoltaic market is dominated by silicon solar cells. One major challenge to achieve high efficiency silicon solar cell is the weak absorption of photons near the band gap of silicon due to its indirect band gap nature. For example the absorption length of silicon drastically increase from 10  $\mu\text{m}$  at the wavelength of 800 nm to 3 mm at 1100 nm. The poor light absorption at the long wavelength region becomes even more severe in thin film solar cells targeting decreased silicon material cost. The solution to boost optical absorption in photovoltaic cells involves design of structures that can strongly trap light within the cell [1]. Various light trapping designs have been proposed and demonstrated during the past few years [2–12]. In particular, periodic diffractive gratings integrated with a backside reflector have been widely recognized as an effective light trapping configuration that can offer absorption enhancement exceeding the classical  $4n^2$  Lambertian limit [13–15]. A metal backside reflector, such as a layer of aluminum, is a popular choice for solar cells, although metallic reflectors suffer for parasitic optical loss due to metal absorption [16]. The other commonly used reflector design is distributed Bragg reflector (DBR) made of alternating high and low-index dielectric layers, which offers high reflectance over its entire photonic stop band [17, 18]. Large index contrast is required for DBR to achieve near-unity omnidirectional reflection, an essential condition for efficient light trapping [19]. Therefore, high-index semiconductors that can be readily deposited into multilayers, such as amorphous silicon (a-Si), are preferred materials for DBR fabrication [17]. Despite the extremely high reflectance of planar DBRs, it was recently found that when gratings are integrated with a DBR, the perfect translational symmetry of the DBR becomes discretized, resulting in zone folding in the reciprocal space (k-space) which closes the DBR photonic band gap, thus allowing light to be scattered into the DBR leading to parasitic optical loss [20].

In this paper, we offer a unified perspective to reveal the origins of optical loss in metal and DBR backside reflector structures integrated with gratings. We start with analyzing the loss mechanism based on the classical coupled mode theory and using DBR as an example. An improved light trapping design is then proposed and numerically validated based on the new insight to mitigate the parasitic loss in DBR, which contributes to further solar cell performance enhancement. Finally, we extend the analysis to metal reflectors and show that

the same design principle applies to suppressing optical loss induced by surface plasmon polariton (SPP) modes.

## 2. Parasitical loss mechanism in DBR integrated with gratings

We note that the photonic zone folding mechanism proposed by Sheng *et al.* can be equivalently accounted for using the classical coupled mode theory. In this new framework, we treat the high-index layers in the DBR as coupled slab waveguides which support in-plane (super) modes. Without gratings, these guided (super) modes can never be accessed from free space as the (in-plane) phase matching condition cannot be satisfied regardless of the light incidence angle. On the other hand, a grating can add integral multiples of its reciprocal lattice basis to the in-plane wave vector of incident light via diffraction. Once the diffracted light phase matches with a guided (super) mode, the light can be efficiently coupled into the DBR and absorbed, which is manifested in the DBR absorption spectrum as a Guided Mode Resonance (GMR) peak. Phase matching condition for the normal incident light is given by:

$$\frac{m \times 2\pi}{\Lambda} = \beta_{gm}, (m \in \mathbb{N}) \quad (1)$$

where  $\Lambda$  denotes the grating period and  $\beta_{gm}$  is the guided mode propagation constant. To validate the phased-matched coupling mechanism, we consider a simplified cell model where the DBR only consists of one bilayer of a-Si and SiO<sub>2</sub> as shown in Fig. 1(a) inset. Since the DBR contains a single high-index layer, the propagation constant of guided mode in the a-Si slab can be analytically solved using classical slab waveguide theory. The wavelength-independent refractive indices of c-Si and a-Si are assumed to be 3.5 and 3.6, respectively, and the extinction coefficients are fixed to 0.1 and 0.01 for c-Si and a-Si, respectively. To facilitate direct comparison with results derived from the zone folding pictures, model parameters consistent with ones reported in [20] were used in our calculations and are listed as follows. The period of grating is set to be 0.8  $\mu\text{m}$ . The c-Si layer is 1.5  $\mu\text{m}$  thick, and is topped with an anti-reflective coating (ARC) made of 70 nm silicon nitride ( $n = 1.8$ ). The DBR is designed to operate at a center wavelength of 800 nm, and the thicknesses of a-Si and SiO<sub>2</sub> layers are determined by the quarter-wave condition ( $\lambda/4n$ ) to be 56 nm and 138 nm, respectively. The numerical simulations are performed using the Rigorous Coupled Wave Analysis (RCWA) method. A convergence study of RCWA parameters was performed to ensure the numerical accuracy. When the number of harmonics is set to 5 with an index resolution of 0.0125, numerical error of the simulated absorption values is within 1%. The wavelength step is fixed at 1 nm for our simulations. Figure 1(a) plots fractional optical absorption in DBR as a function of wavelength. The sharp absorption peak is unequivocally assigned to phase-matched coupling into the guided mode in the DBR. The propagation constant  $\beta$  of the guided mode was calculated to be 23.6  $\mu\text{m}^{-1}$ , which exactly matches  $3 \times 2\pi / 0.8 \mu\text{m}^{-1}$ , the phase factor provided by the gratings' third order diffraction.

## 3. Spacer design for parasitic loss suppression

Based on the k-space description of optical coupling discussed above, we propose an improved back reflector design to minimize light coupling into DBR by inserting a low-refractive-index spacer layer between the grating and the DBR. Even though the addition of the spacer layer does not alter the guided (super) mode structures in the DBR, excitation of these modes are suppressed since diffracted light phase-matched to the guided modes becomes evanescent in the spacer layer ( $\beta_{sp} < \beta_{gm}$ ). The rapid decay of evanescent wave in the spacer layer away from the grating thus effectively prohibits excitation of the guided modes in DBR. Figure 1(b) and 1(c) plot electric field intensity in structures with and without a spacer when the phase matching condition is met. When the spacer is absent, strong coupling into the guided mode is evident; however such coupling is diminished when a spacer is

inserted. The principle is illustrated in Fig. 1(d). As shown in Fig. 1(a), the GMR absorption peak is absent when a 2.5  $\mu\text{m}$  thick spacer layer is added. The slightly higher optical loss background (except the spike) in the structure with spacer is attributed to the formation of a low quality-factor Fabry-Perot cavity between the grating and DBR: the standing wave Fabry-Perot mode is also clearly identified in Fig. 1(c).

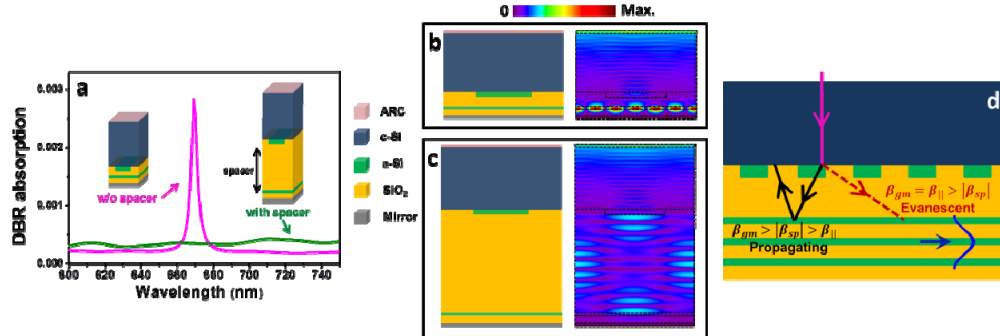


Fig. 1. (a) Optical absorption in the DBR with (green line) and without (magenta line) a spacer layer between the grating and the DBR; (b) and (c) simulated electric field intensity distribution in the cell structures (b) with and (c) without a spacer layer when the phase matching condition is met; (d) schematic illustration of absorption suppression mechanism by adding the spacer layer: the diffraction order phase matched to the guided (super) modes in the DBR and hence responsible for excitation of the guided modes becomes evanescent in the low-index spacer layer, and therefore rapidly decays away from the grating. Consequently, coupling into the guided modes is minimized.

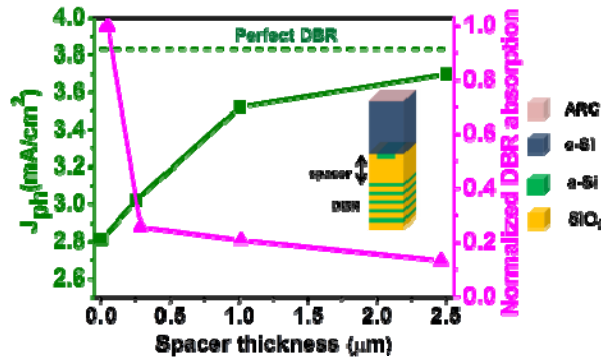


Fig. 2. Influence of spacer layer thickness on integrated photon current (in the wavelength range of 750 nm to 900 nm) and DBR absorption in the thin c-Si solar cell structure analyzed in ([20]).

As an example to show the loss suppression efficacy of our spacer design, we implement the design to further boost light trapping effect and energy conversion efficiency in thin film Si devices compared to the optimized designs presented in [20]. Our simulated performance of thin Si cells is identical to those presented in Fig. 4 from [20]. In our simulations, the DBR consists of 10 bilayers of a-Si and SiO<sub>2</sub>, and the grating period and thickness are optimized with different spacer layer thicknesses, but the DBR design and material constants remain unchanged and are identical to the parameters used in Ref [20]. Clearly, as the spacer layer thickness increases, parasitic absorption in DBR is suppressed, and the photo current  $J_{\text{ph}}$  in the wavelength regime of 750 to 900 nm monotonically increases to 3.7 mA/cm<sup>2</sup>. The horizontal green line in Fig. 2 represents the photo current in cells with lossless/perfect DBR, which stipulates the performance upper limit of our loss mitigation design. In comparison, the optimum back reflector design in Ref [20] yields a  $J_{\text{ph}}$  of 2.9 mA/cm<sup>2</sup> in the same wavelength

range. The significant 30% increase of  $J_{ph}$  is primarily attributed to the reduction of parasitic optical loss in the DBR layers, a trend shown by the magenta line in Fig. 2.

#### 4. Optical loss reduction in planar, unstructured metal reflectors

We note that similar spacer structures were previously used to reduce optical absorption by planar, unstructured backside metal reflectors taking advantage of light trapping by total internal reflection [21–25]. However, unlike DBR, optical absorption in the metal reflectors does not involve guided modes, as surface plasmon polariton modes typically cannot be excited on an unstructured metal surface. Gjessing *et al.* [26] discussed a similar spacer design to mitigate absorption in a back reflector consisting of a metal mirror and a top dielectric grating, although, the authors only presented numerical simulation results without explore on the underlying mechanisms. Holman *et al.* [16] recently identified an interesting case where SPP modes are excited on a planar dielectric-metal interface via evanescent coupling through a thin low-index spacer layer. Their work also unravels the loss suppression mechanism in such configurations.

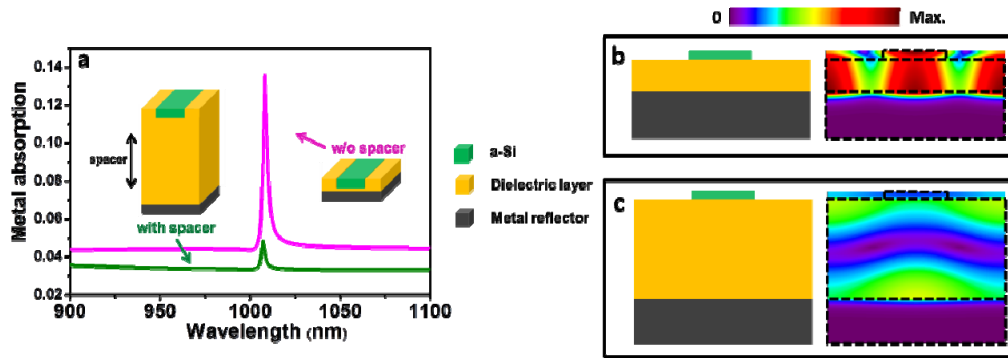


Fig. 3. (a) Optical absorption in the metal reflector with (green line) and without (magenta line) a spacer layer between the grating and the metal reflector; (b) and (c) simulated electric field intensity distribution in the structures shown in Fig. 3(a) inset (b) with and (c) without the spacer layer.

Here we extend our analysis to planar, unstructured metal backside mirrors integrated with dielectric gratings. Figure 3 shows a simplified model that only consists of gratings, a low-index dielectric spacer, and a planar metal layer to analytically validate the phased-matching condition to SPP modes on the metal-dielectric interface. Similar to Eq. (1), the phase matching condition for SPP mode excitation is specified by the equation:

$$\frac{m \times 2\pi}{\Lambda} = \beta_{spp} = \frac{2\pi}{\lambda_0} \sqrt{\frac{\epsilon_d \times \epsilon_m}{\epsilon_d + \epsilon_m}}, (m \in \mathbb{N}) \quad (2)$$

where  $\Lambda$  denotes the grating period and  $\beta_{spp}$  is the propagation constant of surface plasmon polaritons.  $\epsilon_d$  and  $\epsilon_m$  are the permittivity of the dielectric spacer and the metal reflector, respectively. In the simplified example shown in Fig. 3, the complex refractive indices of metal and dielectric layer are chosen to be  $n_m = \sqrt{\epsilon_m} = 1 + 10i$  and  $n_d = \sqrt{\epsilon_d} = 1$ . The absorption peak (magenta line) at  $1.01 \mu\text{m}$  shown in Fig. 3 corresponds to the excitation of SPP mode by the gratings' first order diffraction. According to the phase matching condition (Eq. (2)), the coupling occurs at  $1.01 \mu\text{m}$  wavelength, which perfectly matches our numerical simulation result. Similar to the case of dielectric DBR, as the thickness of dielectric spacer increases from 150 to 450 nm, SPP excitation is minimized, which translates to a major decrease of the SPP absorption peak height (green line) as shown in Fig. 3. The mechanism is

also clearly illustrated in the field distribution plots shown in Figs. 3(b) and 3(c). Unlike the case of DBR, broadband absorption is always present in metal reflectors due to strong material absorption, manifested as the absorption background in Fig. 3. This broadband absorption accounts for the inferior performance of metal mirrors compared to DBR as we will discuss next.

Figure 4 plots photo current enhancement similar to that shown in Fig. 2 when a spacer layer is inserted between metal reflector and solar cell. The Si cell configuration shown in Fig. 4 is identical to that presented in Fig. 2 except that the DBR is replaced with a planar aluminum reflector. As the spacer layer thickness increases, photo current  $J_{ph}$  in the wavelength regime of 750 to 900 nm monotonically increases by 33% from 2.7 mA/cm<sup>2</sup> to 3.6 mA/cm<sup>2</sup>. It is worth noting that the spacer layer thickness should be optimized to minimize optical absorption loss associated with Fabry-Perot resonant modes formed between the grating and reflector as the spacer thickness increases in addition to the guided mode absorption loss. The maximized photo current density (3.6 mA/cm<sup>2</sup>) in Fig. 4 is still lower than that of the optimal design presented in Fig. 2 where DBR is used instead of metal mirrors. This observation indicates the inferior performance of real metal (in this case, aluminum) compared to DBR due to the strong optical absorption in metals. Lastly, we note that lossless/perfect DBR gives identical photo current density (3.83 mA/cm<sup>2</sup>) to from the case of a perfect metal reflector, which suggests that DBR can indeed serve as a perfect omnidirectional broadband reflector for photovoltaic light trapping.

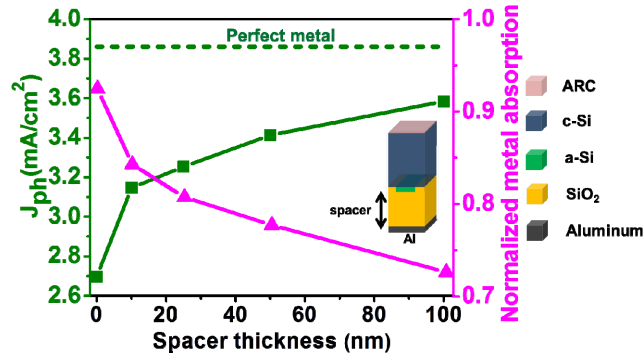


Fig. 4. Influence of spacer layer thickness on integrated photon current (in the wavelength range of 750 nm to 900 nm, green line) and aluminum absorption (magenta line) in the thin c-Si cell structure schematically shown in the inset.

#### 4. Conclusions

In conclusion, we identified phased-matched coupling into guided (super) modes and surface plasmon polariton modes to be key loss contributors in backside dielectric or metal reflectors integrated with diffractive gratings. A spacer design is implemented to minimize excitation of the guided modes and thereby mitigate such parasitic optical loss. While the spacer design is applicable to both dielectric DBR and metal reflectors, we show that DBR exhibits superior light trapping performance given its low inherent material absorption, making it a preferred solution for efficient photovoltaic light trapping provided that a cost-effective multi-layer deposition method can be implemented. Last but not least, while our discussion in this paper focuses on 1-D gratings, the spacer design is also applicable to 2-D gratings, which provide significant light trapping enhancement for both polarizations.

#### Acknowledgments

We acknowledge financial support provided by the Department of Energy under award number DE-EE0005327.